# Hydrologic Model Parameter Estimation in Ungauged Basins using Simulated SWOT Discharge Observations

Nicholas J. Elmer[1], James McCreight[2], Christopher Hain[3]

[1] Science and Technology Institute, Universities Space Research Association, Huntsville, Alabama

[2]National Center for Atmospheric Research, Boulder, Colorado

[3]Earth Science Office, NASA Marshall Space Flight Center, Huntsville, Alabama

Corresponding address: Nicholas J. Elmer, Universities Space Research Association, 320 Sparkman Drive, Huntsville, AL, 35805. Email: nicholas.j.elmer@nasa.gov

Key Points:

- SWOT observations are critical for calibrating hydrologic models in regions devoid of in situ observations
- For an expected SWOT discharge random error of 35%, multi-point parameter estimation is successful for 90% of polar and 60% of tropical sub-basins.
- Multi-point parameter selection is preferred over single-point parameter selection, offering more robust results with less sensitivity.

Keywords: SWOT, WRF-Hydro, Alaska, Parameter Estimation, Calibration

## Abstract

In situ gauge networks are often used in hydrologic model calibration, but these networks are limited or nonexistent in many regions. The upcoming Surface Water Ocean Topography (SWOT) mission promises to fill this observation gap by providing discharge estimates for rivers wider than 100 meters. SWOT observation utility for model parameter selection in regions devoid of in situ gauges is assessed using proxy SWOT discharge estimates derived from an observing system simulation experiment and Monte Carlo methods. The sensitivity of the parameter selection to measurement error and observation frequency is also evaluated. Single- and multi-point parameter selection are performed for ten sub-basins within the Susitna and upper Tanana river basins in Alaska. SWOT is expected to observe Alaskan river points 4-7 times per 21-day repeat cycle with 120-km swath coverage. For an expected SWOT measurement error of 35%, parameter estimation is successful for 50% (90%) of sub-basins using single- (multi-) point parameter selection. Decreasing observation frequency to simulate lower latitudes resulted in success for only 10% of midlatitude and tropical sub-basins for single-point selection, whereas multi-point selection was successful in 80% (60%) of midlatitude (tropical) sub-basins. Single-point parameter selection is more sensitive to measurement error than multi-point parameter selection. The results strongly support the use of multi-point over single-point parameter selection, yielding robust results nearly independent of observation frequency. Most importantly, this study suggests SWOT can be used to successfully select hydrologic model parameters in basins without an in situ gauge network.

## 1. Introduction

For decades, in situ gauge networks have been monitoring stream hydrology and are considered a robust observation with well-understood errors (Hirsch and Costa 2004, Boning 1992), measurements of floods and droughts notwithstanding. Stream gauges aid in the modeling and forecasting of major hydrologic events by enabling model calibration and validation. Unfortunately, in situ stream gauge networks are concentrated to only a few regions globally, and these networks are on the decline (Pavelsky et al. 2014), limiting the availability of observations of streamflow. Furthermore, very few observations are available from satellite platforms since all current satellite missions, including Jason-3 and the second Ice, Cloud and land Elevation Satellite (IceSAT-2), theoretically capable of measuring river stage using radar and laser nadir altimetry (Kouraev et al. 2004, Papa et al. 2010, O'Loughlin et al. 2016, Biancamaria et al. 2017) have insufficient spatial and temporal resolutions for adequate sampling (Alsdorf et al. 2007, Biancamaria et al. 2016).

To fill this observation gap, the Surface Water Ocean Topography (SWOT) mission (Biancamaria et al. 2016) was designed and is expected to be launched in early 2022 to provide the first global inventory of Earth's surface water, including rivers, lakes, and wetlands. A joint venture between the National Aeronautics and Space Administration (NASA), Centre National d'Etudes Spatiales (CNES), Canadian Space Agency, and the United Kingdom Space, SWOT supports a nadir altimeter and a bistatic Ka-band (35.75 GHz) Radar Interferometer (KaRIn) (Fjortoft et al. 2014). The nadir altimeter allows intercomparison with Jason measurements, will help to continue the data record of nadir altimeters, and fills the gap between the two 60 km KaRIn swaths, one on each side of nadir. KaRIn provides high-resolution water surface elevation (WSE, the height of the river surface above a reference geoid), width, and slope measurements across a

combined 120 km swath for rivers wider than 100 m (Biancamaria et al. 2016, Pavelsky et al. 2014, Rodriguez 2016). Since KaRIn uses Ka-band, instead of C- and Ku-band used by Jason and IceSAT, there is less signal penetration into soil, snow, and vegetation (Fjortoft et al. 2014, Biancamaria et al. 2016) enabling SWOT to collect measurements at finer spatial resolutions. Therefore, KaRIn will be the first satellite instrument that can fully resolve terrestrial surface water bodies with high altimetric accuracy.

In the United States (U. S.), U. S. Geological Survey (USGS) stream gauges measure river stage at 3 mm accuracy, which translates to discharge accuracy of 5-10% (Hirsch and Costa 2004) under normal flow conditions. Generally, a 1% error in the effective stage input is equivalent to a 3% error in the computed discharge (Boning 1992). In comparison, SWOT WSE is expected to have a minimum error of 10 cm for most rivers (Biancamaria et al. 2016) with estimated discharge errors around 35% (Durand et al. 2016). However, even though expected SWOT errors are much larger than the error of in situ gauges, in the absence of in situ gauges SWOT measurements will provide the best estimates of stage and discharge available. This work also highlights that SWOT observations along many points in the stream network have better error characteristics than a single observation, as errors between sites are not assumed to be correlated.

Hydrologic models, including the National Oceanic and Atmospheric Administration (NOAA) National Water Model (NWM; OWP 2020) which is an instantiation of the Weather Research and Forecasting Hydrological extension package (WRF-Hydro; Gochis et al. 2018), are typically calibrated using in situ gauges. WRF-Hydro is a modeling framework that couples column land surface, overland and subsurface terrain routing, and channel routing models in a multiscale hydrologic process representation. WRF-Hydro is fully-distributed with multi-physics options and multi-scale capabilities, enabling it to represent processes on a wide range of spatial

scales (Yucel et al. 2015, Senatore et al. 2015, Arnault et al., 2018, Gochis et al. 2018). Since many parameterizations are used to characterize sub-scale processes in numerical models, parameter values are often hard-coded or contained in parameter tables. For example, 139 hard-coded parameters and 71 standard parameters were identified within Noah-MP by Cuntz et al. (2016). Running Noah-MP coupled with WRF-Hydro, Cuntz et al. (2016) found that hydrologic output fluxes are sensitive to two-thirds of the standard parameters and surface runoff is sensitive to many parameters of snow processes, soil, and vegetation. Even after calibration, many parameter values can vary widely from basin to basin, even between neighboring watersheds. Calibration seeks to minimize an objective function as a measure of physical realism by optimizing the parameter values of the most sensitive model parameters.

Few, if any, alternatives are available if *in situ* observations are lacking. Following launch, SWOT will provide an additional source of discharge observations from a satellite platform, potentially providing more observations per basin than even some of the most robust in situ networks. This paper assesses the ability of SWOT discharge estimates to enable hydrological model parameter selection in regions devoid of in situ gauges. This paper also compares multi-point parameter selection (e.g., Cao et al. 2006, Niraula et al. 2012), which will be made possible with SWOT observations, to the traditional single-point calibration approach. Previous multi-point calibration studies use robust gauge networks for their analysis, but in situ gauges have substantially lower observation error and higher temporal sampling than is expected of SWOT. Thus, this study is essential in understanding whether single- and multi-point parameter selection can be performed solely using SWOT observations. A related study, Nickles et al. (2020), compared hydrologic model multi-site calibration results using daily stream gauge observations, SWOT temporally-sampled discharge (no uncertainty), and SWOT temporally-sampled discharge

with uncertainty (systematic and random error), finding that SWOT achieves similar calibration results to in situ daily observations. However, this study differs from Nickles et al. (2020) by expanding results beyond the mid-latitudes and investigating the sensitivity of parameter selection to a potential range of SWOT measurement error.

## 2. Methodology

### 2.1 Experimental Design

The design of our fraternal twin parameter selection experiment is shown in Figure 1. This Observing System Simulation Experiment (OSSE) is based on Elmer et al. (2020a,b). The fraternal twins, the "truth run" and "calibration run", simulate model error by employing different hydrologic model representations in the model chain that generates streamflow. The experiment addresses whether the unknown, best parameters for the calibration run can be reliably selected (purple box in Figure 1) from observations of the truth run streamflow imparted with the expected observation error characteristics of the SWOT sensor. Successfully identifying the best parameters from observations is the core of model calibration. In this experiment, because we know the true streamflow values, we can evaluate under what conditions parameter selection is successful.

Parameter, model, and observation errors are all ingredients of the experimental design. The parameter error is the quantity we seek to minimize in parameter selection and calibration via the objective function. The truth run was pre-calibrated to a single subdomain of the study and has a single realization (yellow box, Figure 1). In contrast, the calibration runs span the space of thirteen model parameters plus Manning's roughness coefficient using 80 parameter sets. This is represented by the stack of calibration runs (red boxes) in Figure 1. Model error of the calibration runs relative to the truth run is generated by differences summarized by text in the respective boxes

in Figure 1. These differences produce errors between the runs in terms of 1) the fixed boundary conditions or geometry for different land surface model (LSM) resolutions and channel routing networks, 2) the LSM and channel parameters, particularly infiltration parameters, which depend on spatial and temporal model resolutions, and 3) streamflow physics. We note that both the atmospheric forcing variables and LSM models are identical between the runs but that errors or differences in the model runs start with and accumulate over time within the soil moisture representation and its two-way coupling to the overland and subsurface runoff models (Gochis and Chen 2003), which feeds back to LSM behavior and parameter differences. The differences between the fraternal twins are described in further detail below.

The SWOT observation (discharge) errors are considered both systematic (biased) and random. 10,000 realizations of observation errors are applied to the true states before use in parameter selection to avoid drawing conclusions from a particular set of random errors. This set of 10,000 possible observation realizations is represented by the stack of observations (blue ovals) in Figure 1. Although results using as few as 1000 realizations would have led to similar conclusions, 10,000 realizations are used for this study to ensure robust results. The use of 10,000 realizations is also consistent with other studies (e.g., Nickles et al. 2020). Over the 10,000 observation sets, the probability of selection (identification as the best parameter set via a version of Nash-Sutcliffe Efficiency (NSE; McCuen et al. 2006) based on the observations) is computed for each of the 80 parameter sets (purple diamond, Figure 1). Finally, in the evaluation step (green diamond, Figure 1), NSE is computed from the true model states and the true rank of each parameter set is assigned, from best (low) to worst (high). The cumulative probability of parameter selection (under observation error) is plotted against rank. Do the true best parameter sets have a

156 reasonably high likelihood of selection in the presence of SWOT observation characteristics (and
157 model error)?

158 This paper focuses on sub-basins within the upper Tanana River and Susitna River basins
159 in Alaska, which will be regularly observed by SWOT (Biancamaria et al. 2016) but have few in
160 situ observations. These watersheds are delineated in Figure 2. The following subsections provide
161 additional details for each step of the experimental design shown in Figure 1.

162

163 2.2 Model configurations and parameters

164 For both truth and calibration model runs in Figure 1, this study uses WRF-Hydro version
165 5.0 (Gochis et al. 2018) configured to mimic the NWM v2.0 configuration (OWP 2020). The Noah
166 land surface model with Multi-Parameterization options (Noah-MP; Niu et al. 2011) with a 1 km
167 spatial resolution is used as the WRF-Hydro land surface model in both models, as well as Global
168 Land Data Assimilation System (GLDAS) Version 2 (Rodell et al. 2004) meteorological forcing.
169 Further details of the model configuration and physics parameterizations used are listed in Table
170 1, which also lists the differences between the truth run and the calibration runs.

171 The truth (calibration) run configuration has a model timestep of 1 (3) hours, performing
172 overland and subsurface routing on a 100m (250m) grid, and uses the Muskingum-Cunge
173 (diffusive wave) routing scheme for simulating streamflow within a channel model. GLDAS
174 forcing data is available at three-hour increments and ingested into both configurations equally.
175 The WRF-Hydro terrain routing grids (100m and 250m) and channel networks were derived from
176 the WRF-Hydro GIS Pre-processing Toolkit v5.1 (Sampson and Gochis 2015) using the Weather
177 Research and Forecasting (WRF; Skamarock et al. 2008) Preprocessing System geogrid file and
178 the National Elevation Dataset (NED; U. S. Geological Survey 2017) Digital Elevation Model

(DEM) as inputs. Both the Muskingum-Cunge and diffusive wave schemes represent channels with an infinite depth, preventing overbank flow. However, the diffusive wave scheme allows backwater effects, whereas the Muskingum-Cunge scheme does not. Importantly, the channel networks are derived using different DEM spatial resolutions, leading to different spatial representations of the channel routing.

Whereas we calibrate the truth run to in situ streamflow observations (described below), the calibration run configuration is uncalibrated: the point of our experiment being selection of parameters for the calibration run that most accurately simulate the truth run. Eighty calibration parameter sets were created by perturbing Manning's roughness coefficient (as a function of stream order) along with the thirteen most sensitive WRF-Hydro parameters (Cuntz et al. 2016; Elmer 2019). As shown in Table 2, these parameters span the LSM, overland/subsurface routing, groundwater bucket, and channel routing components of the model (model variable names shown in parentheses): the Clapp-Hornberger B exponent (bexp), soil moisture maximum (smcmax), saturated soil conductivity (dksat), soil infiltration parameter (refkdt), soil drainage parameter (slope), retention depth (RETDEPRTFAC), saturated soil lateral conductivity (LKSATFAC), groundwater bucket model max depth (Zmax), groundwater bucket model exponent (Expon), canopy wind parameter (CWPVT), maximum carboxylation at 25°C (VCMX25) which is related to the vegetation height (HVT), the Ball-Berry conductance relationship slope (MP), and the snowmelt parameter (MFSNO). The ranges assigned to these parameters make up the calibration parameter space. From this parameter space, a sample of parameter sets were obtained by randomly assigning values within the valid parameter ranges listed in Table 2 using a uniform distribution. The result is a good representation of parameter space, as shown by depiction of the distribution of the sampled parameter sets using a multidimensional scaling (MDS) transform (Pedregosa et

al. 2011) in Figure 3. MDS is a method by which distances in multi-dimensional space (in this case, a thirteen-dimensional parameter space) are transformed to two-dimensional distances while maintaining the true distance in the original multi-dimensional space as closely as possible.

The truth model is calibrated using in situ USGS stream gauge observations at the basin outlet using the parameter space described above (Table 2). The mean of the linear NSE and the logarithmic NSE ($NSE_{ln}$) was used as the calibration metric, denoted as the mean NSE ($NSE_{mean}$). $NSE_{mean}$ is akin to the metric used in the calibration of the NWM and is given by:

$$NSE_{mean} = (w)NSE + (1 - w)NSE_{ln} \qquad (1)$$

where w is the weight of 0.5. $NSE_{mean}$ ranges from negative infinity to unity, where a value greater than zero indicates that the model provides a better estimate than the observation mean. Thus, the maximum $NSE_{mean}$ is sought. For single point parameter selection, $NSE_{mean}$ is the metric for evaluation. For multipoint parameter selection, a basin average $NSE_{mean}$ is calculated for evaluation, given by:

$$\overline{NSE_{mean}} = \frac{\sum_{i=1}^{P} NSE_{mean_i}}{P} \qquad (2)$$

where P is the number of observed points in the sub-basin or watershed.

As the calibration process is computationally expensive, calibration of the truth simulation was only performed for the Chena River watershed (within the upper Tanana River basin; watershed outlet denoted by point I in Figure 2) and halted after 75 model iterations. The parameters identified using the Chena River calibration were transferred to the full domain. Although the Chena River calibration may not transfer well to the entire upper Tanana River and Susitna River basins, the resulting model output is treated as truth for this experiment and therefore a perfect calibration is not necessary. Certain parameters (e.g., infiltration parameters) are strongly scale dependent, so the calibration of the truth model, in which the model resolution and

streamflow physics differ from the 250-m model, is not directly transferrable to the 250-m model. The truth run provides the "true" geolocation and discharge time series (q) for the purposes of this experiment.

A spin-up period of eight years (March 2009 - March 2017) using default parameter values (Table 2) was performed, designed to allow for adequate accumulation of groundwater and snowpack and permitting each 250-m simulation to reach equilibrium. The March 2017 restart files from the spin-up were used to restart the 250-m simulations at March 2011 using their respective parameter set and integrated forward in time in an open loop configuration. The periods of March – September 2012 for the Susitna River basin and March – September 2014 for the upper Tanana River basin were used during analysis to determine the utility of SWOT observations in model parameter selection.

### 2.3. Generating Proxy SWOT Discharge

Since real SWOT data are not yet available, proxy SWOT observations were generated for this analysis. Proxy SWOT data have been used by multiple studies to quantify assimilation impacts on river modeling and reservoir management (Andreadis et al. 2007; Biancamaria et al. 2011, Munier et al. 2015; Emery et al. 2020; Revel et al. 2021; Yang et al. 2019; Wongchuig-Correa et al. 2020) and develop procedures for estimating river bathymetry (Durand et al. 2008, 2010, 2014; Yoon et al. 2012). Furthermore, Pedinotti et al. (2014) used synthetic SWOT data to optimize Manning roughness coefficients in the Interactions between Soil, Biosphere, and Atmosphere-Total Runoff Integrating Pathways System (ISBA-TRIP) continental hydrologic system using data assimilation, demonstrating that SWOT data can be used for calibration.

The truth model q is corrupted with random and systematic error following a Gaussian distribution (N) with mean β and standard deviation $\epsilon$:

$$q' = q\big(1 + N(\beta, \epsilon)\big), \qquad (3)$$

where $q = (q_{i,t_0}, q_{i,t_1}, \dots, q_{i,t_n})$ is a discharge time series for the i-th channel reach, $q'$ is the corrupted discharge (i.e., the proxy SWOT discharge estimate), β is the relative bias, and $\epsilon$ is the relative discharge error. For the analysis in Section 3.1, $\epsilon = 0.35$ is used, which is roughly equivalent to the relative root mean squared error (RMSE) of instantaneous discharge estimated by Durand et al. (2016). β is constant with time for each q, but varies in space (across channel reaches). Since an equivalent increase in water surface height will yield a larger increase in discharge for a river with a larger cross-section, uncertainty in *q'* naturally increases as q increases.

However, a single series of *q'* does not provide an adequate sampling of random error and bias by which to assess calibration potential. Rather, it gives a snapshot of only one possible scenario. Figure 4 illustrates this point. The blue dots indicate a single time series of *q'*, containing some points in which the discharge random errors are small and depart very little from the truth value but also points that extend into the 2-σ error range. A single scenario may be skewed if only small random errors are present ($q' \approx q$), especially at key points along the time series, which would enable superior parameter selection and suggest better results than could actually be expected. Conversely, a scenario containing frequent large errors, parameter selection would underperform. To sample a broad spectrum of the possible outcomes stemming from a SWOT observation set laden with error, Monte Carlo methods were employed to create 10,000 randomly-perturbed sets of *q'* per sub-basin. Thus, each of the 10,000 error realizations of *q'* is characterized by random white noise ($\epsilon$) and time-constant systematic bias ($\beta$), where the value of β is randomly drawn from N(0.00, 0.20) based on Hagemann et al. (2017) to account for relative bias prior to

applying Eq. (3). Following the creation of the 10,000 sets, the probability of successful sub-basin parameter selection was calculated.

To obtain *q'* with appropriate orbit characteristics, it was spatially sampled based on the CNES proxy SWOT orbit (Aviso+ 2015) with a simulated start date of 1 March 2012. First, the cross-track distance of each WRF-Hydro reach from the proxy SWOT orbit at each overpass was calculated. For each pass, only reaches with cross-track distances of 10-60 km (i.e., within the SWOT measurement range) and with a Strahler streamorder greater than or equal to five (used to approximate rivers with widths greater than 50 m) were extracted, following the methodology of Elmer et al. (2020a), which showed that Alaskan rivers with a streamorder greater than or equal to five will generally be observable by SWOT. Figure 3 compares the truth *q* and *q'* for sub-basin E, where *q'* is used to calibrate the 250-m model following the method described in Section 2.3.

## 2.3. Parameter selection from proxy SWOT discharge observations

We purposely use the term "parameter selection" to differentiate our overall approach from calibration for the following reasons. The parameter sets run through the model and ultimately judged by the objective function are generated a priori through combinations of uniformly sampled distributions on each parameter. As such, the parameters sets being discriminated via the objective function are generally not "close" in parameter space (Figure 3). A true calibration approach would consider points with a similar spacing in parameter space, but would also include parameter sets much closer together in the quest to find minima of the objective function. This paper does not study the ability to accurately find local minima of the objective function using SWOT observations. Doing so would require understanding the relative sensitivities of the objective function to observation error and to distance in parameter space. Rather, we examine the potential

for SWOT observations to give a more regional, less detailed picture of the objective function. Given the observation and error characteristics of SWOT, including its spatially distributed nature, and a finite collection of parameter sets, can we accurately select the best parameter set in this collection? Our results provide an encouraging basis for pursuing model calibration using SWOT observations.

To review and summarize the experiment design (Figure 1), the 250-m model described in Section 2.1 represents an uncalibrated hydrologic model of an ungauged basin (a single red box, Figure 1). For this basin, an infinite number of parameter sets can be selected from the parameter space for calibration and the correct solution (parameter set) is unknown. The goal is to find the best simulation of streamflow over a finite sample of parameter space. A sample size of 80 parameter sets (red stack of boxes, Figure 1) was chosen for this study to minimize computational requirements. While the parameter set can certainly be expanded to more fully represent the whole parameter space, the increased computational requirements may reduce the feasibility of this method for users without access to large computing systems.

This study ensures the 250-m model is blind to the calibration of the truth model so that the calibrated parameter set used by the truth model does not inform the selection of the parameter set sampling for the 250-m model. In the absence of in situ gauges, the only source of regular discharge observations for ungauged basins will be from the SWOT mission. The $q'$ values derived in Section 2.3 are representative of the SWOT discharge observations that will be available post-launch, and are used to calibrate the model by finding the best parameter set from the 80 sample parameter sets. A comparison between the 100-m truth model, the 250-m simulations, and the proxy SWOT discharge estimates is provided in Table 3, with example data shown in Figure 4.

For this particular point, there are 38 SWOT overpasses from March 1 – September 15, yielding an observation approximately every 5 days, or 4 observations per repeat cycle.

Channel reaches were spatially matched between the truth and calibration model channel networks for evaluation, eliminating any matches separated by a 1 km or greater which are considered unrelated. Thus, a total of 10 basins and 991 channel reaches were evaluated. All basins were modeled simultaneously, but evaluated separately. Single-point parameter selection for the uncalibrated 250-m model is performed using $NSE_{SWOT}$, given as the $NSE_{mean}$ between the discharge for each simulation and $q'$ at each sub-basin outlet in Figure 2. Multi-point parameter selection is evaluated with $\overline{NSE_{SWOT}}$, the basin average $NSE_{SWOT}$ for all observed points P (Equation 2). The 250-m simulation with the maximum $NSE_{SWOT}$ or $\overline{NSE_{SWOT}}$ (the best match parameter set) is chosen, and the parameter set used by that simulation for the thirteen most sensitive WRF-Hydro parameters is selected as the "correct" parameter set.

## 2.4. Evaluation of parameter selection

The $NSE_{mean}$ was also calculated between each 250-m simulation and the truth model q ($NSE_{TRUTH}$) at each basin outlet for comparison with $NSE_{SWOT}$ for single point parameter selection evaluation. Multi-point parameter selection is similar to single-point selection except that $\overline{NSE_{SWOT}}$ and $\overline{NSE_{TRUTH}}$ (the basin-average values for all observable channel reaches within each sub-basin) is used. The 250-m simulations are separately ranked according to their $NSE_{SWOT}$ ($\overline{NSE_{SWOT}}$) and $NSE_{TRUTH}$ ($\overline{NSE_{TRUTH}}$) values for single point (multi-point) parameter selection with the member with the best (maximum) value being assigned a ranking of one, and the member with the worst (minimum) value assigned a ranking of 80. Expressing the cumulative rank of $NSE_{SWOT}$ ($\overline{NSE_{SWOT}}$) as a function of $NSE_{TRUTH}$ ($\overline{NSE_{TRUTH}}$) reveals whether single (multi) point

parameter selection using SWOT observations is effective. For the purpose of drawing conclusions in this paper, a successful parameter selection is achieved for a watershed if the selected parameter set is contained within the best ten sets according to the $NSE_{TRUTH}$ ($\overline{NSE_{TRUTH}}$) rank with a >80% probability. This criteria is subjective, thus plots showing the full range of probabilities are included. For example, in Figure 5a the y-axis shows the cumulative probability whereas the x-axis shows the parameter set rank. The cumulative probability is essentially the fraction of observation sets (10,000 sets in total). Thus, we see that for sub-basin G (pink line), approximately 0.90 (90%) of the 10,000 observation sets rank the true best parameter set in the top ten (indicated by vertical black dashed line). Since this value is above the 0.8 (80%) threshold, the parameter selection is successful.

## 2.5 Sensitivity to measurement error and temporal frequency

Additional analysis examines the sensitivity of the parameter selection results to measurement error (Section 3.2) and the temporal frequency of SWOT observations (Section 3.3). Although the measurement error of SWOT instantaneous discharge is estimated to have a relative RMSE of 35%, this error may be higher (Hagemann et al. 2017; Durand et al. 2016). Conversely, the incorporation of ancillary data in the discharge algorithms or using a multialgorithm approach may reduce error further (Durand et al. 2016). Thus, determining the sensitivity of these results to measurement error is useful in evaluating the range of possible impacts for SWOT, in particular with respect to model calibration. Thus, $q'$ is calculated with $\epsilon$ values of 0.0, 0.2, 0.35, 0.5, 0.75, and 1.0. The temporal frequency of SWOT observations is inherently tied to latitude due to SWOT orbit characteristics (relatively narrow swath compared to satellite imagers and high inclination angle). Thus, polar regions are observed more frequently than the midlatitudes, and the

midlatitudes are observed more frequently than the tropics. Biancamaria et al. (2016) show that SWOT will observe the tropics (0-30°) 1-2 times per repeat cycle, the midlatitudes (30-60°) 2-4 times per repeat cycle, and polar regions (60-90°) 3-7 times per repeat cycle.

To assess the sensitivity of parameter selection results to temporal frequency and determine whether this process is viable at lower latitudes, the same Alaskan sub-basins are considered but the observation frequency of *q'* is reduced to mimic SWOT observation of mid- and low-latitudes basins. For the midlatitudes, the observation frequency of *q'* was halved with respect to that of Alaska. For the tropics, the observation frequency was reduced by a factor of four. The sensitivity of model parameter selection to measurement error and the temporal frequency of observations is calculated by:

$$S = \frac{\partial Y}{\partial X}, \qquad (4)$$

where Y is the probability of selection and X is the measurement error ε or number of observations per repeat cycle.

## 3. Results and discussion

### 3.1. Parameter selection

Figure 5a presents the cumulative probability that the true best parameter set is selected via $NSE_{SWOT}$ at or above (equal or higher ranking) each rank position for a random error $\epsilon$=0.35 using single-point parameter selection. For example, if the rank 10 likelihood for a given basin is 80%, then the parameter set selected by $NSE_{SWOT}$ is one of the ten highest-ranked sets with respect to the truth for 8,000 of the 10,000 Monte Carlo simulations. For five of the ten sub-basins, the selected parameter set is ranked in the top ten with a >80% probability, meeting our criteria for success. These five sub-basins plus sub-basin I also rank in the top five with a >60% probability.

Notably, two sub-basins (B and D) display much poorer results than the other sub-basins. Sub-basin B selects a parameter set in the top 50 with less than a 30% probability, indicating that the best parameter set as determined by $NSE_{TRUTH}$ is poorly ranked by this parameter selection approach. Sub-basins B and D experience substantial diurnal oscillations in streamflow presumably due to snowmelt during the warm season resulting in a flashy hydrograph. Table 4 provides the Richards-Baker Flashiness Index (R-B Index; Baker et al. 2004) for each sub-basin as a quantitative measure of basin flashiness. Although daily discharge is typically used in the calculation, Baker et al. (2004) suggests the use of hourly discharge when diurnal oscillations are significant, thus hourly discharge is used in the calculation in Table 4. These results suggest that SWOT is not well-suited for parameter selection or calibration in basins with rapidly changing discharge, as the sporadic nature of the SWOT temporal sampling along with measurement uncertainty does not allow a good sampling of the truth hydrograph. Consequently, even the best parameter set has a poor $NSE_{SWOT}$, making it difficult to extract the correct parameter set using this methodology.

Figure 6 compares the $NSE_{TRUTH}$ for each sub-basin shown in Figure 2. The $NSE_{TRUTH}$ curves for both B and D are flatter than for the other sub-basins, indicating that the sample parameter set spread is narrower. Thus, there is less variation among the simulations, resulting in lower ranked parameter sets based on $NSE_{TRUTH}$ to be more frequently ranked highly based on $NSE_{SWOT}$. Additionally sub-basin B has the lowest $NSE_{TRUTH}$ of any sub-basin for its highest ranked set with a value less than 0.75. Figure 7 maps the true rank of each parameter set selected by $NSE_{SWOT}$ and displays a histogram of these ranks for all SWOT observable channel reaches in the domain. Results are generally very good for the entire upper Tanana basin and most of the Susitna basin, with the selection of a highly-ranked (top 10) parameter set for most of the channel

reaches. However, the worst performance occurs in the same outlying sub-basins B and D from Figure 6, with sub-basin B clearly demonstrating the poorest results. Thus, in addition to poor SWOT sampling, it is also apparent that the simulation does not capture the physical processes of these flashy sub-basins as well as for the other sub-basins, indicating that the sample parameter set does not contain the true parameter set and resulting in the inability to achieve a good parameter selection using the approach in this paper. However, this shortcoming highlights several potential issues with parameter selection. Adequate model spin-up and configuration are necessary to ensure significant physical processes are being adequately captured by the model and that physical realism is adequate. Second, parameter sets which appropriately cover the parameter space may also be key to differentiating model simulations (Sharma et al. 2019, Hagedorn et al. 2012, Weigel et al. 2008, 2009). A larger parameter set or a parameter sampling strategy that undertakes large searches across parameter space may benefit the parameter selection at several sites in this study.

Figure 8a, interpreted in the same manner as Figure 5a, presents the cumulative probability of successful parameter selection for a random error $\epsilon = 0.35$ using multi-point parameter selection. Results improve compared to single-point parameter selection. For nine out of ten (90%) of the sub-basins, the selected parameter set has a true rank in the top ten with a >80% probability, meeting our criteria for successful parameter selection. The only sub-basin that again does not achieve successful calibration is sub-basin B for the same reasons as discussed above. Six basins also identify parameter sets in the top five true parameter sets with >60% probability.

### 3.2. Sensitivity to measurement error

Reducing the discharge random error ε from 0.35 to 0.20 results in the success probabilities shown in Figures 5b and 8b for single-point and multi-point parameter selection, respectively. As

expected, the probability that the selected parameter set is highly ranked increases as random error decreases, with the exception of sub-basin B for reasons discussed in Section 3.1. For single-point parameter selection (Fig. 5b), 50% of sub-basins are assigned a top-ten ranked parameter set with a >95% cumulative probability, while 70% of sub-basins meet the definition of successful parameter selection. 60% of sub-basins also display a >80% probability of selecting a parameter set ranked in the top five. These statistics are improved further using multi-point parameter selection (Fig. 8b) with 90% of sub-basins achieving successful parameter selection and 70% of sub-basins with a >95% cumulative probability. Figure 9 summarizes the effect of decreasing $\epsilon$, showing that as random error decreases the likelihood of successful parameter selection generally increases, regardless of observation frequency. However, decreasing $\epsilon$ below 0.35 does not yield improved results for multi-point parameter selection except for the tropics, suggesting that systematic bias is the predominant factor in preventing successful parameter selection when $\epsilon$ is less than 0.35. Conversely, as $\epsilon$ increases above 0.35 the likelihood of successful parameter selection quickly drops regardless of observation frequency with single (multi-) point parameter selection being successful for 0% (40%) of sub-basins for $\epsilon = 0.50$.

The sensitivity of the probability of successful parameter selection is evaluated by considering a 0.10 decrease in observation random error ε within the 0.20 – 0.50 range. The mean sensitivity is calculated over all channel reaches. The mean sensitivity for each rank position is shown in Figure 10 with single-point and multi-point selection sensitivity as blue dashed and solid lines, respectively. For single-point parameter selection, the probability is most sensitive at ranks 9-13, with a maximum sensitivity over 6% per 0.10 decrease in $\epsilon$. Sensitivity gradually declines for ranks beyond 13, which is to be expected since the cumulative probability, as shown in Figure 5, begins to level off for lower rank positions for most sub-basins. For multi-point parameter

selection, random error sensitivity peaks at rank 7 with a maximum sensitivity over 7% per 0.10 decrease in $\epsilon$, and rapidly decreasing beyond rank 7. The use of multi-point parameter selection yields a slightly more robust result parameter selection, as the sensitivity is lower than single-point parameter selection at the rank 10 threshold. This is further supported by Figure 9, in which an increase in $\epsilon$ from 0.20 – 0.50 results in a smaller reduction in success for multi-point compared to single point parameter selection. For both single- and multi-point parameter selection, a sizeable improvement in success can be expected if the SWOT observation error can be reduced through the use of ancillary datasets.

### 3.3 Sensitivity to temporal frequency of SWOT observations

Single-point parameter selection is very sensitive to the temporal frequency of SWOT observations. As shown in Figure 9, for $\epsilon = 0.35$ successful parameter selection is reduced from 60% (polar) to 10% (tropics) of sub-basins, whereas for $\epsilon = 0.20$ it is reduced from 70% of polar to 30% of tropical sub-basins. For multi-point parameter selection, probability of success is reduced from 90% to 50% of sub-basins for $\epsilon = 0.35$ and from 90% to 70% of sub-basins for $\epsilon = 0.20$ for the same reduction in observation frequency. Figure 11 compares the cumulative probability curves for the midlatitudes and the tropics using multi-point parameter selection, which alongside Figure 8a, shows that 60% of sub-basins were largely unaffected by the four-fold decrease in observation frequency.

The sensitivity due to a single additional SWOT observation per repeat cycle for each rank position is shown in Figure 10 with single-point and multi-point parameter selection identified by the orange dashed and solid lines, respectively. In calculating sensitivity to observation frequency, five observations per repeat cycle (21 days) is assigned to the polar region, three observations per

repeat cycle is given to the midlatitudes, and 1.5 observations per repeat cycle is used for the tropics. For example, in calculating sensitivity between the polar region and tropics, $\partial X = 5 - 1.5 = 3.5$. The magnitudes and patterns are similar to that of observation error sensitivity. For single-point parameter selection, maximum sensitivity is observed between ranks 7-10, peaking near 5% per additional observation. For multi-point parameter selection, sensitivity peaks at 2% but drops to approximately 1% beyond rank 10. Clearly, while the number of SWOT observations per repeat cycle noticeably affects the likelihood of successful parameter selection using single-point parameter selection, multi-point selection is much more robust. Similar success using multi-point parameter selection is achieved for polar regions, midlatitudes, and tropics for the full range of evaluated $\epsilon$. Further, a large majority of sub-basins achieved successful parameter selection regardless of observation frequency for $\epsilon \leq 0.35$, demonstrating that reduced observation error can compensate for lower observation frequency.

## 4. Conclusions

Using Monte Carlo methods, we evaluate parameter selection for an uncalibrated 250-m WRF-Hydro model. We examine single- and multi-point objective function parameter selection using simulated SWOT observations in regions unserved or underserved by in situ gauges. The model parameter space is sampled to create an assortment of parameter sets for which the 250-m model is run. Proxy SWOT discharge estimates were derived from an OSSE following the methodology of Elmer et al. (2020a, b). As the true values of streamflow are known, we can evaluate the selection of model parameters based on the comparison of model discharge simulations with proxy SWOT streamflow observations.

The results indicate that the use of multi-point parameter selection is advantageous over single-point parameter selection. In effect, the spatially distributed nature of the SWOT observations compensates for systematic and random nature of observation error. In fact, successful parameter selection is largely independent of random error for $\epsilon \leq 0.35$. The high spatial coverage of observations from SWOT also compensates for the lack of their temporal frequency in mid-latitude and tropical basins, perhaps due to spatiotemporal correlations in streamflow (Paiva et al. 2015, Yang et al. 2019, Fisher et al. 2020). Further, this study finds that SWOT can successfully be used for hydrologic model parameter selection despite the non-uniform space-time sampling, agreeing with Nickles et al. (2020). However, whereas Nickles et al. (2020) results are constrained to mid-latitude river basins, this study finds that this conclusion applies to nearly the full range of SWOT temporal sampling. Even with larger errors than in situ gauges, this study shows that SWOT discharge estimates can provide adequate accuracy and temporal sampling to enable parameter selection for SWOT observable river basins globally with the exception of basins experiencing significant variability (flashy basins). In regions devoid of in situ observations or with relatively scarce stream gage networks, this study demonstrates that SWOT will provide valuable observations for calibrating hydrologic models.

This study does not account for reprocessing of discharge estimates occasionally throughout the SWOT mission, which is a planned activity to improve accuracy. Actual SWOT observations are expected by mid-2022, so these results are timely in preparing to apply SWOT data immediately following launch. While SWOT has many societal and research applications that rely on near-real-time SWOT measurements (e.g., data assimilation, inundation mapping), the use of SWOT observations for model parameter selection or calibration is not constrained by product latency or mission lifetime, but extend beyond the mission end.

*Acknowledgements.* This work was funded by NASA Headquarters under the NASA Postdoctoral Program at NASA Marshall Space Flight Center administered by Universities Space Research Association. All software and input data to run WRF-Hydro can be obtained freely online and are cited in the references. Data used in analysis and the creation of figures are available at doi: 10.5281/zenodo.4434565. The authors thank Michael Durand and two anonymous reviewers for providing useful and constructive comments that contributed to overall quality of the paper.

## References

Alsdorf, D. E., E. Rodriguez, and D. P. Lettenmaier (2007), Measuring surface water from space, Rev. Geophys., 45, RG2002, doi:10.1029/2006RG000197.

Anderson, J. T., T. Hoar, K. Raeder, H. Liu, N. Collins, R. Torn, and A. Avellano (2009), The Data Assimilation Research Testbed: A community facility, Bull. Amer. Meteor. Soc., vol. 90, pp. 1283-1296, doi:10.1175/2009BAMS2618.1.

Andreadis, K. M., E. A. Clark, D. P. Lettenmaier, and D. E. Alsdorf (2007), Prospects for river discharge and depth estimation through assimilation of swath-altimetry into a raster-based hydrodynamics model, Geophys. Res. Lett., 34(L10403), 1-5, doi:10.1029/2007GL029721.

Arnault, J., S. Wagner, T. Rummler, B. Fersch, J. Bliefernicht, S. Andresen, and H. Kunstmann (2016), Role of Runoff–Infiltration Partitioning and Resolved Overland Flow on Land–Atmosphere Feedbacks: A Case Study with the WRF-Hydro Coupled Modeling System for West Africa. J. Hydrometeor., 17, 1489–1516, doi:10.1175/JHM-D-15-0089.1.

Aviso+ (2015), SWOT orbit, https://www.aviso.altimetry.fr/en/missions/future-missions/swot/orbit.html, accessed 8 September 2015.

Baker, David B., R. Peter Richards, Timothy T. Loftus, and Jack W. Kramer, 2004. A New Flashiness Index: Characteristics and Applications to Midwestern Rivers and Streams. Journal of the American Water Resources Association (JAWRA) 40(2):503-522.

Biancamaria., S., M. Durand, K. M. Andreadis, P. D. Bates., A. Boone, N. M. Mognard, and E. A. Clark (2011), Assimilation of virtual wide swath altimetry to improve Arctic river modeling, Remote Sens. Environ., 115(2), 373-381, doi:10.1016/j.rse.2010.09.008.

Biancamaria, S., F. Frappart, A.-S. Leleu, V. Marieu, D. Blumstein, J. D., Desjonqueres, F. Boy, A. Sottolichio, and A. Valle-Levinson (2016), Satellite radar altimetry water elevations performance over a 200 m wide river: Evaluation over the Garonne River, Advances in Space Research, 59(2017), 128-146, doi:10.1016/j.asr.2016.10.008.

Biancamaria, S., F. Frappart, A.-S. Leleu, V. Marieu, D. Blumstein, J. D., Desjonqueres, F. Boy, A. Sottolichio, and A. Valle-Levinson (2017), Satellite radar altimetry water elevations performance over a 200 m wide river: Evaluation over the Garonne River, Advances in Space Research, 59(2017), 128-146, doi:10.1016/j.asr.2016.10.008.

Boning, C. W., (1992), Policy statement on stage accuracy. Tech. rep., Office of Surface Water Technical Memorandum No. 93.07, available at https://water.usgs.gov/admin/memo/SW/sw93.07.html.

Cao, W., W. B. Bowden, T. Davie, and A. Fenemor (2006), Multi-variable and multi-site calibration and validation of SWAT in a large mountainous catchment with high spatial variability. Hydrol. Process., 20, 1057-1073, doi:10.1002/hyp.5933.

Cunge, J. A. (1969), On the subject of a flood propagation computation method (Muskingum method), J. Hydraul. Res., 7, 205-230.

Cuntz, M., J. Mai, L. Samaniego, M. Clark, V. Wulfmeyer, O. Branch, S. Attinger, and S. Thober (2016), The impact of standard and hard-coded parameters on the hydrologic fluxes in the Noah-MP land surface model, J. Geophys. Res. Atmos., 121, 10,676–10,700, doi:10.1002/2016JD025097.

Durand, M. K., K. M. Andreadis, D. E. Alsdorf, D. P. Lettenmaier, D. Moller, and M. Wilson (2008), Estimation of bathymetric depth and slope from data assimilation of swath altimetry into a hydrodynamic model. Geophys. Res. Lett., 35 (L20401), 1-5, doi:10.1029/2008GL034150.

Durand, M., E. Rodriguez, D. E. Alsdorf, and M. Trigg (2010), Estimating river depth from remote sensing swath interferometry measurements of river height, slope and width, IEEE. J. Sel. Top. Appl. Earth Observ. Remote Sens., 3(1), 20-31, doi:10.1109/JSTARS.2009.2033453.

Durand, M., J. Neal, E. Rodriguez, K. M. Andreadis, L. C. Smith, and Y. Yoon (2014), Estimating reach-averaged discharge for the River Severn from measurements of river water surface elevation and slope, J. Hydrol., 5111, 92-104, doi:10.1016/j.jhydrol.2013.12.050.

Durand, M., et al. (2016), An intercomparison of remote sensing river discharge estimation algorithms from measurements of river height, width, and slope, Water Resour. Res.,52, 4527–4549, doi:10.1002/2015WR018434.

Emery, C. M., Biancamaria, S., Boone, A., Ricci, S., Rochoux, M. C., Pedinotti, V., & David, C. H.(2020). Assimilation of wide-swath altimetry water elevation anomalies to correct large-scale river routing model parameters. Hydrology and Earth System Sciences, 24(5), 2207- 2233. https://doi.org/10.5194/hess-24-2207-2020

590 Elmer, N. J. (2019), Using satellite observations of river height and vegetation to improve
591 National Water Model initialization and streamflow prediction, Ph.D. dissertation,
592 Department of Earth and Atmospheric Science, The University of Alabama in Huntsville,
593 Huntsville, Alabama, 113 pp, available online at
594 https://cdm16608.contentdm.oclc.org/digital/collection/p16608coll23/id/64232.
595 Elmer, N. J., C. R. Hain, F. Hossain, D. Desroches, C. Pottier (2020a), Generating proxy SWOT
596 water surface elevations using WRF-Hydro and the CNES SWOT Hydrology Simulator,
597 Water Resour. Res., Early Online Release, doi:10.1002/essoar.10502399.1.
598 Elmer, N. J., C. Hain, J. McCreight, D. Gochis (2020b), SWOT Applications for WRF-Hydro
599 Modeling in Alaska, IGARSS 2020 - 2020 IEEE International Geoscience and Remote
600 Sensing Symposium, pp. 5077-5080, doi: 10.1109/IGARSS39084.2020.9323136.
601 Fisher, C. K., M. Pan, and E. F. Wood (2020), Spatiotemporal assimilation-interpolation of
602 discharge records through inverse streamflow routing, Hydro. Earth. Syst. Sci., 24, 293-
603 305, doi:10.5194/hess-24-293-2020.
604 Fjørtoft R, Gaudin JM, Pourthie N, Lalaurie JC, Mallet A, Nouvel JF, Martinot-Lagarde J, Oriot
605 H, Borderies P, Ruiz C, Daniel S (2014), KaRIn on SWOT: characteristics of near-nadir
606 Ka-band interferometric SAR imagery. IEEE Trans Geosci Remote Sens 52(4):2172–
607 2185, doi:10.1109/TGRS.2013.2258402.
608 Gochis, D.J., M. Barlage, A. Dugger, K. FitzGerald, L. Karsten, M. McAllister, J. McCreight, J.
609 Mills, A. RafieeiNasab, L. Read, K. Sampson, D. Yates, W. Yu, (2018). The WRF-Hydro
610 modeling system technical description, (Version 5.0). NCAR Technical Note. 107 pages.
611 Available online at https://ral.ucar.edu/sites/default/files/public/WRF-
612 HydroV5TechnicalDescription.pdf. Source Code DOI:10.5065/D6J38RBJ.

Gochis, D.J. and F. Chen, 2003: Hydrological enhancements to the community Noah land surface model. NCAR Technical Note, NCAR/TN-454+STR, 68 pp.

Hagedorn, R., Buizza, R., Hamill, T. M., Leutbecher, M., and Palmer, T. (2012). Comparing TIGGE multimodel forecasts with reforecast-calibrated ECMWF ensemble forecasts. Quarterly Journal of the Royal Meteorological Society, 138(668), 1814–1827.

Hagemann, M.W.; Gleason, C.J.; Durand, M.T. BAM: Bayesian AMHG-Manning Inference of Discharge Using Remotely Sensed Stream Width, Slope, and Height. Water Resour. Res. 2017, 53, 9692–9707, doi:10.1002/2017WR021626.

Hirsch, R. and J. E. Costa (2004), U.S. streamflow measurement and data dissemination improve. Eos Trans. AGU, 85 (20), 197-203, doi:10.1029/2004EO200002.

Kouraev, A. V., E. A. Zakharova, O. Samain, N. M. Mognard, and A. Cazenave (2004), Ob river discharge from TOPEX/Poseidon satellite altimetry (1992–2002), Remote Sens. Environ., 93, 238-245.

McCuen, R. H., Z. Knight, and A. G. Cutter (2006), Evaluation of the Nash–Sutcliffe efficiency index, J. Hydrol. Eng., 11(6), 597–602, doi:10.1061/(ASCE)1084-0699(2006)11:6(597).

Munier, S., A. Polebistki, C. Brown, G. Belaud, and D. P. Lettenmaier (2015), SWOT data assimilation for operational reservoir management on the upper Niger River Basin, Water Resour. Res., 51, 554-575, doi:10.1002/2014WR016157.

Nickles, C., Beighley, E., & Feng, D. (2020). The Applicability of SWOT's Non-Uniform Space-Time Sampling in Hydrologic Model Calibration. Remote Sensing, 12(19), 3241. https://doi.org/10.3390/rs12193241.

634 Niraula, R., L. M. Norman, T. Meixner, and J. B. Callegary (2012), Multi-gauge calibration for
635 modeling the semi-arid Santa Cruz watershed in Arizona-Mexico border area using
636 SWAT. Air, Soil and Water Research, 5, 41-57, doi:10.4137/ASWR.S9410.
637 Niu, G.-Y., Z.-L. Yang, K. E. Mitchell, F. Chen, M. B. Ek, M. Barlage, A. Kumar, K. Manning,
638 D. Niyogi, E. Rosero, M. Tewari, and Y. Xia (2011), The community Noah land surface
639 model with multiparameterization options (Noah-MP): 1. Model description and
640 evaluation with local-scale measurements, J. Geophys. Res., 116(D12109),
641 doi:10.1029/2010JD015139.
642 O'Loughlin, F. E., J. Neal, D. Yamazaki, and P. D. Bates (2016), ICESat-derived inland water
643 surface spot heights, Water Resour. Res., 52, 3276-3284, doi:10.1002/2015WR018237.
644 OWP (cited 2020), The National Water Model, http://water.noaa.gov/about/nwm.
645 Paiva, R. C. D., M. T. Durand, and F. Hossain (2015), Spatiotemporal interpolation of discharge
646 across a river network by using synthetic SWOT satellite data, Water Resour. Res., 51,
647 430–449, doi:10.1002/2014WR015618.
648 Papa, F., F. Durand, W. B. Rossow, A. Rahman, and S. K. Bala (2010), Satellite altimeter-
649 derived monthly discharge of the Ganga-Brahmaputra River and its seasonal to
650 interannual variations from 1993 to 2008, J. Geophys. Res., 115(C12013),
651 doi:10.1029/2009JC006075.
652 Pavelsky, T. M., M. T. Durand, K. M. Andreadis, R. E. Beighley, R. C. D. Paiva, G. H. Allen,
653 and Z. F. Miller (2014), Assessing the potential global extent of SWOT river discharge
654 observations, J. Hydrol., 519, 1516-1525, doi:10.1016/j.jhydrol.2014.08.044.
655 Pedinotti, V., A. Boone, S. Ricci, S. Biancamaria, and N. Mognard (2014), Assimilation of
656 satellite data to optimize large-scale hydrological model parameters: a case study for the

SWOT mission, Hydrol. Earth Syst. Sci., 18, 4485-4507, doi:10.5194/hess-18-4485-2014.

Pedregosa, F., Varoquaux, G., Gramfort, A., Michel, V., Thirion, B., Grisel, O., et al. (2011). Scikit-learn: Machine Learning in Python. Journal of Machine Learning Research, 12(85), 2825–2830

Revel, M., Ikeshima, D., Yamazaki, D., & Kanae, S. (2021). A framework for estimating global-scale river discharge by assimilating satellite altimetry. Water Resources Research, 57, e2020WR027876. https://doi.org/10.1029/2020WR027876

Rodell, M., P. R. Houser, U. Jambor, J. Gottschalck, K. Mitchell, C.-J. Meng, K. Arsenault, B. Cosgrove, J. Radakovich, M. Bosilovich, J. K. Entin, J. P. Walker, D. Lohmann, and D. Toll (2004), The Global Land Data Assimilation System, Bull. Amer. Meteor. Soc., 85(3), 381-394.

Rodriguez, E. (2016), Surface Water and Ocean Topography Mission (SWOT) Project, Science Requirements Document, Rev A, 28 pp., https://swot.jpl.nasa.gov/files/swot/D-61923_SRD_Rev%20A_20160318%20with%20signatures1.pdf.

Sampson, K. and D. Gochis (2015), WRF-Hydro GIS pre-processing tools: Version 2.2 documentation, Tech. rep., Boulder, Colorado, 39 pages.

Senatore, A., G. Mendicino, D. J. Gochis, W. Yu, D. N. Yates, and H. Kunstmann (2015), Fully coupled atmosphere-hydrology simulations for the central Mediterranean: Impact of enhanced hydrological parameterization for short and long time scales, J. Adv. Model. Earth Syst., 7, 1693-1715, doi:10.1002/2015MS000510.

678 Sharma, S., Siddique, R., Reed, S., Ahnert, P., and Mejia, A. (2019). Hydrological model
679 diversity enhances streamflow forecast skill at short- to medium-range timescales. Water
680 Resources Research, 55, 1510–1530, doi:10.1029/2018WR023197.
681 Skamarock, W. C., J. B. Klemp, J. Dudhia, D. O. Gill, D. M. Barker, M. G. Duda, X.-Y. Huang,
682 W. Wang, and J. G. Powers (2008), A description of the Advanced Research WRF
683 version 3, NCAR Technical Note, 475, 113 pp.,
684 http://www2.mmm.ucar.edu/wrf/users/docs/arw_v3.pdf.
685 U. S. Geological Survey (2017), National Elevation Dataset (NED),
686 https://nationalmap.gov/elevation.html.
687 Weigel, A. P., Liniger, M., and Appenzeller, C. (2008). Can multi-model combination really
688 enhance the prediction skill of probabilistic ensemble forecasts? Quarterly Journal of the
689 Royal Meteorological Society, 134(630), 241–260.
690 Weigel, A. P., Liniger, M. A., and Appenzeller, C. (2009). Seasonal ensemble forecasts: Are
691 recalibrated single models better than multimodels? Monthly Weather Review, 137(4),
692 1460–1479.
693 Wongchuig-Correa, S., de Paiva, R. C. D., Biancamaria, S., & Collischonn, W. (2020).
694 Assimilation of future SWOT-based river elevations, surface extent observations and
695 discharge estimations into uncertain global hydrological models. Journal of Hydrology,
696 590, 125473.
697 Yang, Y., Lin, P., Fisher, C. K., Turmon, M., Hobbs, J., Emery, C. M., et al. (2019). Enhancing
698 SWOT discharge assimilation through spatiotemporal correlations. Remote Sensing of
699 Environment, 234, 111450. https://doi.org/10.1016/j.rse.2019.111450

700 Yang, Y., C. Fisher, and J. T. Reager (2019), Enhancing SWOT discharge assimilation through
701 spatiotemporal correlations, Remote Sensing of Environment, 234, 111450,
702 doi:10.1016/j.rse.2019.111450.
703 Yoon, Y., M. Durand, C. J. Merry, E. A. Clark, K. M. Andreadis, and D. E. Alsdorf (2012),
704 Estimating river bathymetry from data assimilation of synthetic SWOT measurements, J.
705 Hydrol., 464-465, 363-375, doi:10.1016/j.jhydro.2012.07.028.
706 Yucel, I., A. Onen, K. K. Yilmaz, and D. J. Gochis (2015), Calibration and evaluation of a flood
707 forecasting system: Utility of numerical weather prediction model, data assimilation, and
708 satellite-based rainfall, J. Hydrol., 523, 49-66, doi:10.1016/j.jhydrol.2015.01.042.
709

## List of Tables

## List of Figures

742 Figure 8. Same as Figure 5, but for multi-point parameter selection showing results for a) ε=0.35
743 and b) ε=0.20.
744 Figure 9. Probability of successful single and multi-point parameter selection (%) for each
745 latitude zone as a function of relative measurement error (ε).
746 Figure 10. Mean sensitivity (% change per unit) of the probability that the selected parameter set
747 is ranked at or above each rank position with respect to changes in proxy SWOT discharge
748 error ε (blue) and SWOT observation frequency (orange) for single-point (dashed) and multi-
749 point (solid) parameter selection. Since error sensitivity is likely non-linear, note that this
750 evaluation should not be extrapolated beyond 0.20 – 0.50. Units are shown in the legend in
751 parentheses, and rank is determined by $NSE_{TRUTH}$ and $\overline{NSE_{TRUTH}}$. The vertical dashed line
752 marks the 10th-ranked member.
753 Figure 11. As in Figure 8a, but for proxy SWOT mimicking observation frequency for a)
754 midlatitudes and b) tropics as opposed to Alaska. Results are for multipoint parameter
755 selection.
756

## Tables

Table 1. Noah-MP and WRF-Hydro parameterization options used. More information about these options is available in Niu et al. (2011) and Gochis et al. (2018).

| Noah-MP Namelist Option | Namelist Value |
|---|---|
| Dynamic Vegetation Option | 4 (table leaf area index, maximum GVF) |
| Canopy Stomatal Resistance Option | 1 (Ball-Berry) |
| BTR Option | 1 (Noah) |
| Runoff Option | 3 (free drainage) |
| Surface Drag Option | 1 (M-O) |
| Frozen Soil Option | 1 (linear effects) |
| Supercooled Water Option | 1 (no iteration) |
| Radiative Transfer Option | 3 (two-stream applied to vegetated fraction) |
| Snow Albedo Option | 2 (CLASS) |
| PCP Partition Option | 1 (Jordan 1991) |
| TBOT Option | 2 (original Noah) |
| Temp Time Scheme Option | 3 (semi-implicit) |
| Glacier Option | 2 (original Noah) |
| Surface Resistance Option | 4 (Sakaguchi and Zeng for non-snow, snow surface resistance for snow) |
| WRF-Hydro | |
| Channel Routing Option | Truth run: 2=Muskingum-Cunge,<br>Calibration runs: 3=Diffusive Wave (gridded) |
| Overland Flow Routing Option | 1 (D8) |
| Groundwater/Baseflow Routing Option | 1 (Exponential Bucket) |
| Resolutions | |
| LSM Timestep | Truth run: 1 hr<br>Calibration runs:3 hr |
| LSM Spatial | 1 km |
| Overland/Suburface Spatial | Truth: 100 m<br>Calibration runs: 250 m |

762 Table 2. Parameter table listing the model parameters comprising parameter space. The listed value
763 was applied either as a multiplicative factor (Mult) or as an absolute (substituted) value (Abs).

| Component | Parameter (Variable name) | Variable name | Scaling | Minimum Value | Maximum Value | Default value |
|---|---|---|---|---|---|---|
| LSM | Clapp-Hornberger B exponent | bexp | Mult | 0.4 | 1.9 | 1.0 |
| | Soil moisture maximum | smcmax | Mult | 0.8 | 1.2 | 1.0 |
| | Saturated soil conductivity | dksat | Mult | 0.2 | 10.0 | 1.0 |
| | Soil infiltration parameter | refkdt | Abs | 0.1 | 4.0 | 0.6 |
| | Soil drainage parameter | slope | Abs | 0.0 | 1.0 | 0.1 |
| | Canopy wind parameter | CWPVT | Mult | 0.5 | 2.0 | 1.0 |
| | Maximum carboxylation at 25°C | VCMX25 | Mult | 0.6 | 1.4 | 1.0 |
| | Ball-Berry conductance relationship slope | MP | Mult | 0.6 | 1.4 | 1.0 |
| | Snowmelt parameter | MFSNO | Abs | 0.5 | 3.5 | 2.0 |
| Overland/ subsurface | Retention depth | RETDEPRTFAC | Abs | 0.1 | 10.0 | 1.0 |
| | Saturated soil lateral conductivity | LKSATFAC | Abs | 10 | 10 000 | 1000 |
| Bucket | Groundwater bucket maximum depth | Zmax | Abs | 10 | 250 | 25 |
| | Groundwater bucket exponent | Expon | Abs | 1.0 | 8.0 | 1.75 |
| Channel | Manning's roughness coefficient | MannN | Abs | **Minimum** | **Maximum** | **Default** |
| | | | **Order** | **Value** | **Value** | **value** |
| | | | 1 | 0.45 | 0.65 | 0.55 |
| | | | 2 | 0.25 | 0.45 | 0.35 |
| | | | 3 | 0.125 | 0.25 | 0.15 |
| | | | 4 | 0.085 | 0.125 | 0.10 |
| | | | 5 | 0.060 | 0.085 | 0.07 |
| | | | 6 | 0.045 | 0.060 | 0.05 |
| | | | 7 | 0.035 | 0.045 | 0.04 |
| | | | 8 | 0.025 | 0.035 | 0.03 |
| | | | 9 | 0.015 | 0.025 | 0.02 |
| | | | 10 | 0.005 | 0.015 | 0.01 |

764

765 Table 3. Comparison between truth model, 250-m model, and proxy SWOT time series.

| | Truth (100-m) model | 250-m model | Proxy SWOT |
|---|---|---|---|
| **Overland Routing Spatial Resolution** | 100 m | 250 m | Not Applicable |
| **Channel Routing Scheme** | Muskingum-Cunge (vector) | Diffusive Wave (gridded) | Not Applicable |
| **Temporal Resolution** | 1-hour | 3-hour | Irregular |
| **Calibration** | Based on Chena River watershed calibration using USGS gauges | Uncalibrated | Not Applicable |
| **Sets** | 1 | 80 | 10,000 |

766

767 Table 4. Richards-Baker Flashiness Index (R-B Index) for each sub-basin calculated using

768 hourly discharge from the analysis period.

| Sub-basin | R-B Index |
|---|---|
| A | 0.66 |
| B | 2.02 |
| C | 0.76 |
| D | 1.30 |
| E | 0.66 |
| F | 0.26 |
| G | 1.06 |
| H | 0.90 |
| I | 0.54 |
| J | 0.20 |

769

## Figures

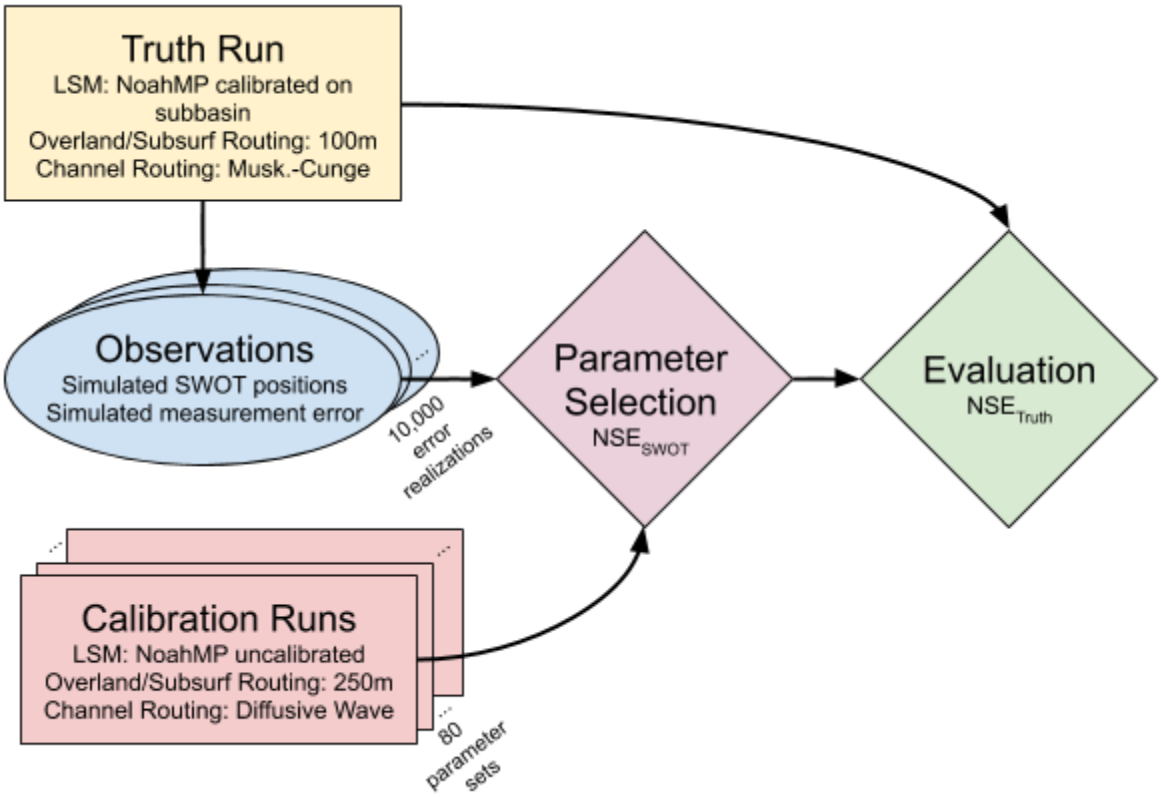


Figure 1. Design of "fraternal twin" experiment for evaluating the utility of (simulated) SWOT for hydrologic parameter selection with the WRF-Hydro model: Do the space-time sampling and observation error characteristics of SWOT permit accurate calibration?

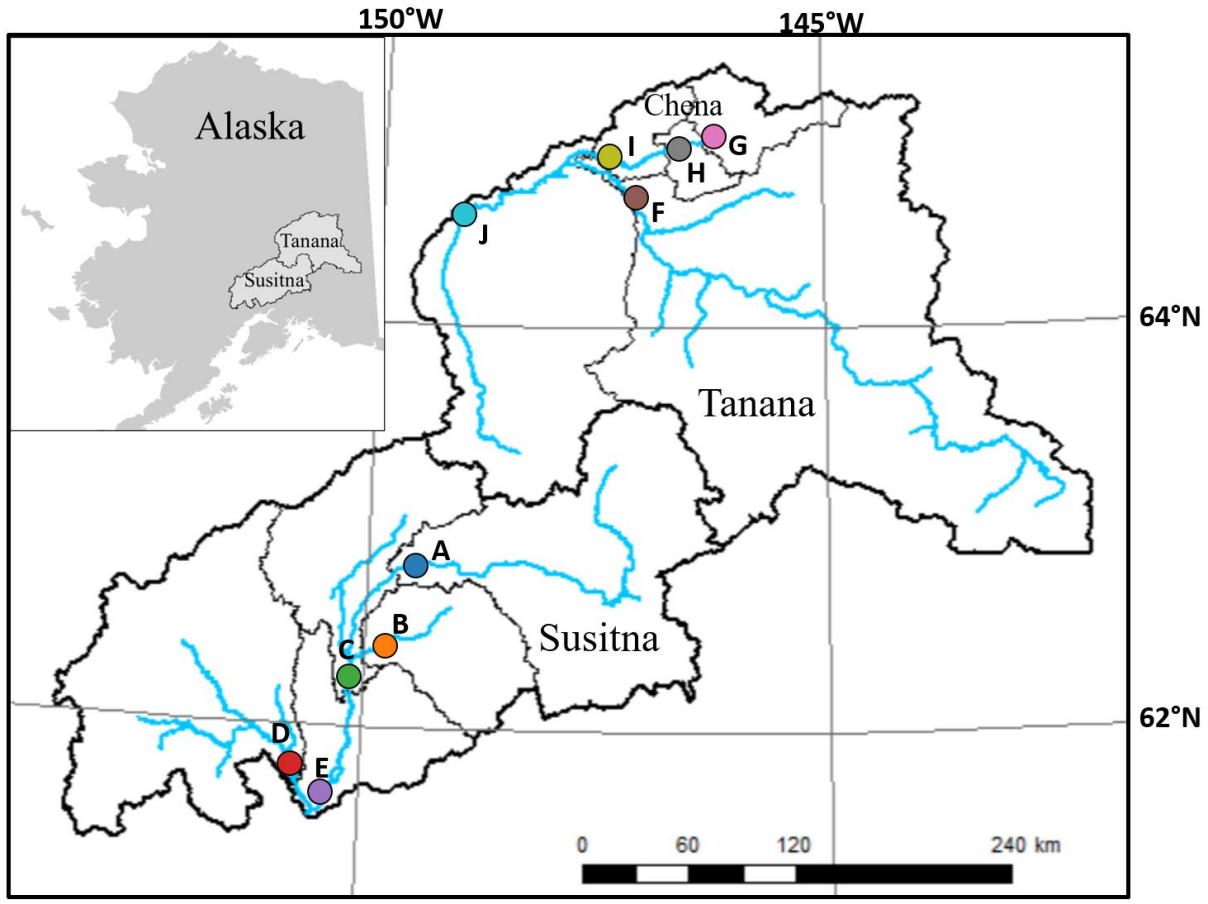


Figure 2. Study area within the Susitna River and upper Tanana River basins. The letters indicate sub-basins A-J with colors corresponding with Figure 5. Streams of order five and greater are designated in blue.

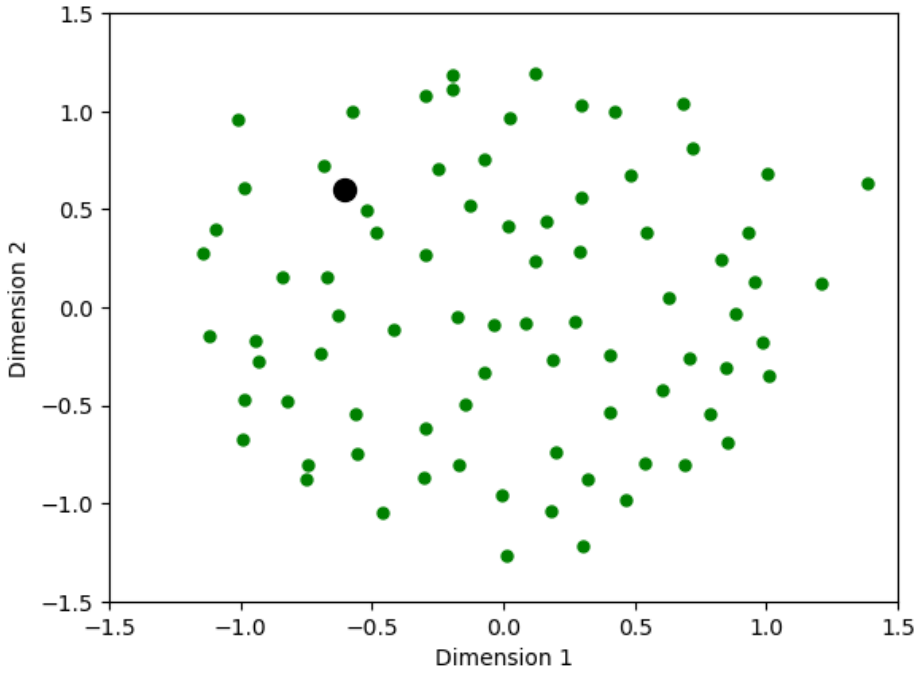


Figure 3. Distribution of the sampled parameter sets (green) used in this study visualized using two-dimensional multidimensional scaling. These dimensions are generically labeled as they do not readily correspond to the original parameter space. For reference, the calibrated parameter set for the truth model is shown in black.

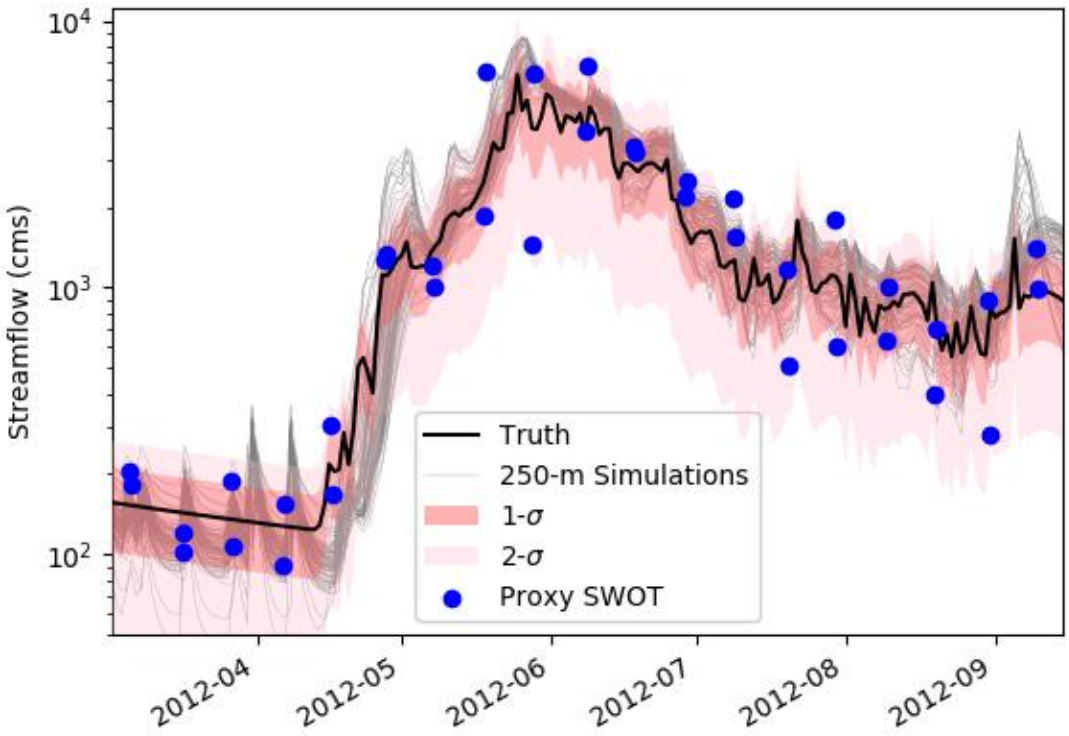


787

788 Figure 4. 250-m simulations, truth simulation, 1-σ and 2-σ discharge error ranges, and a sample

789 proxy SWOT discharge observation set (i.e., hydrograph) for a single point corresponding to the

790 sub-basin E outlet.

791

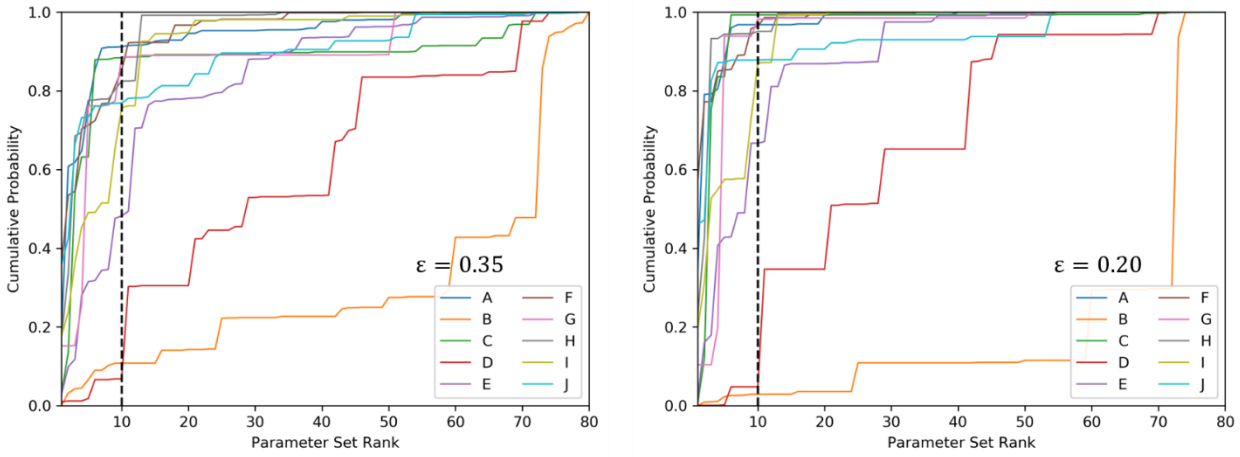


(a) (b)

Figure 5. Percent of sub-basins with successful single-point parameter selection for a given cumulative probability and parameter set rank for a discharge error ε of a) 0.35 and b) 0.20. Rank is determined by $NSE_{TRUTH}$. The vertical dashed line marks the 10th-ranked member.

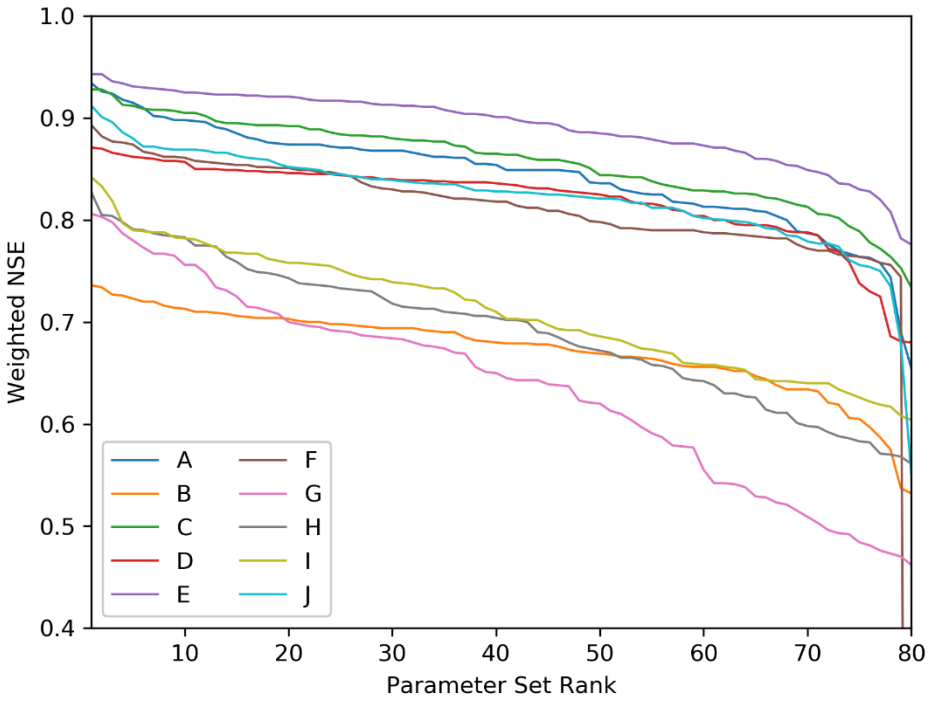


Figure 6. $NSE_{TRUTH}$ for each point A-J in Figure 2. Parameter set rank is determined by $NSE_{TRUTH}$ at the basin outlet (single-point).

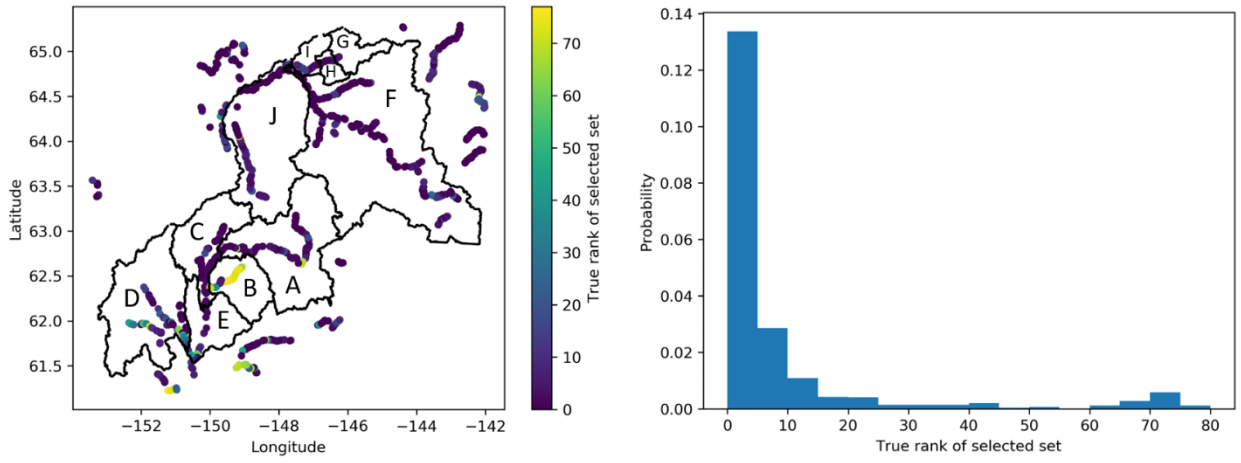


(a) (b)

Figure 7. a) Map and b) histogram depicting the true rank of selected parameter set for $\epsilon = 0.35$ in Alaska. All SWOT observable channel reaches are shown. Basin borders match those in Figure 2. Zero indicates the best true rank.

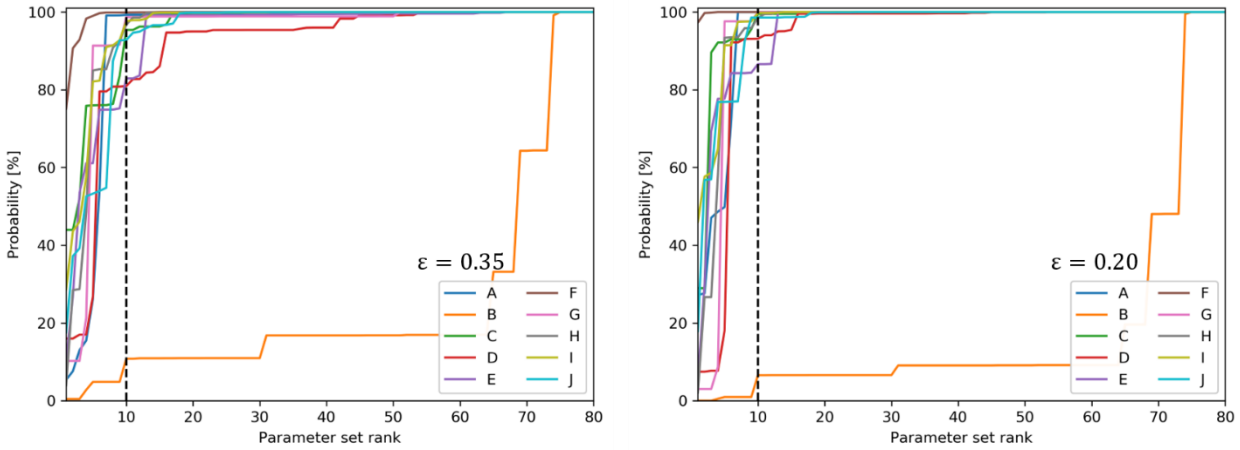


(a) (b)

Figure 8. Same as Figure 5, but for multi-point parameter selection showing results for a) ε=0.35 and b) ε=0.20.

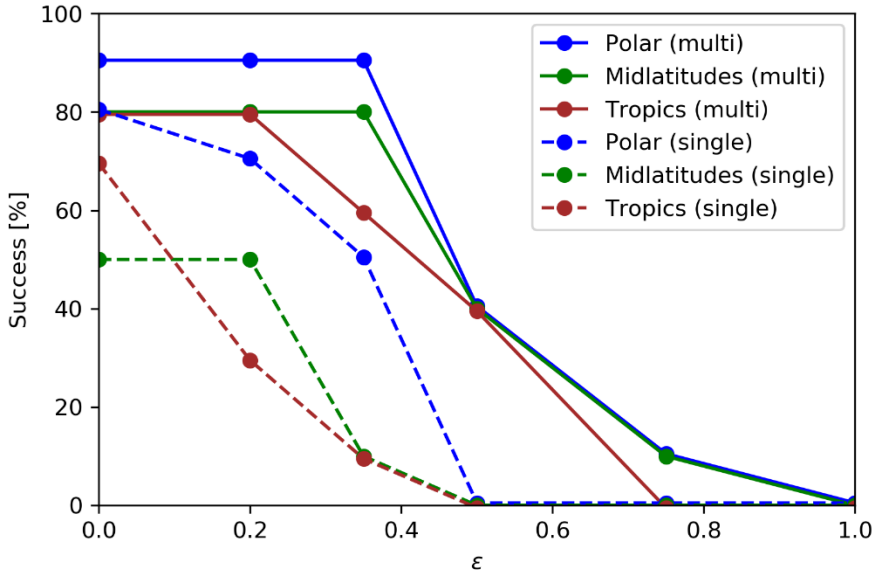


Figure 9. Probability of successful single and multi-point parameter selection (%) for each latitude zone as a function of relative measurement random error (ε).

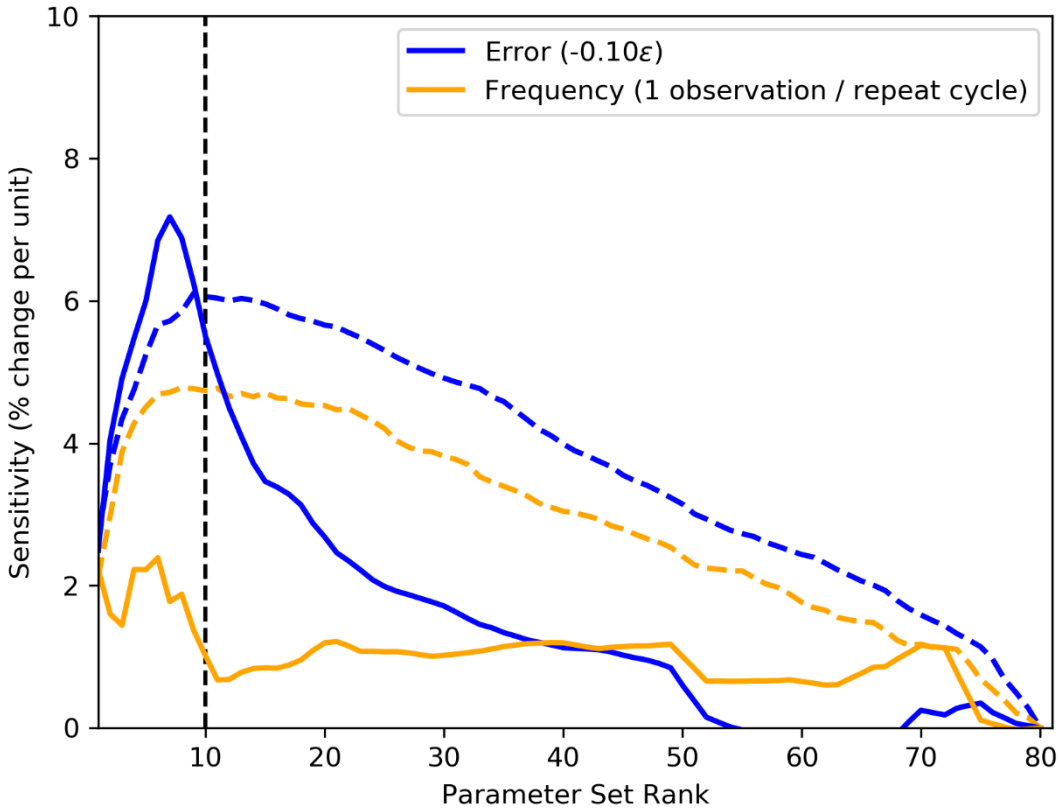


Figure 10. Mean sensitivity (% change per unit) of the probability that the selected parameter set is ranked at or above each rank position with respect to changes in proxy SWOT discharge error ε (blue) and SWOT observation frequency (orange) for single-point (dashed) and multi-point (solid) parameter selection. Since error sensitivity is likely non-linear, note that this evaluation should not be extrapolated beyond 0.20 – 0.50. Units are shown in the legend in parentheses, and rank is determined by $NSE_{TRUTH}$ and $\overline{NSE_{TRUTH}}$. The vertical dashed line marks the 10th-ranked member.

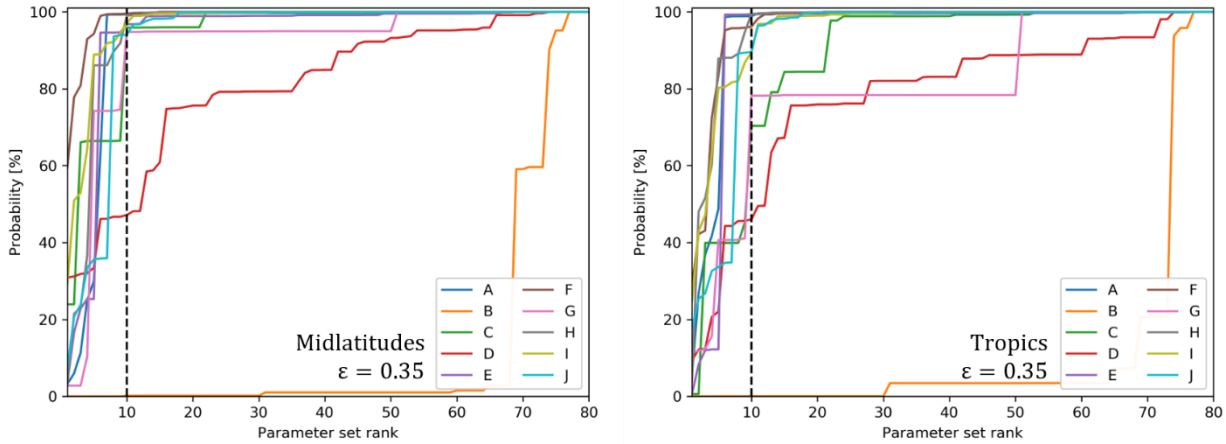


(a) (b)

Figure 11. As in Figure 8a, but for proxy SWOT mimicking observation frequency for a) midlatitudes and b) tropics as opposed to Alaska. Results are for multipoint parameter selection.